*Q. J. R. Meteorol. Soc.* (1997), **123**, pp. 1961–1984

# Convergence zones over the Greek peninsula and associated thunderstorm activity

By VASSILIKI KOTRONI*, GEORGE KALLOS and KONSTANTINOS LAGOUVARDOS
*University of Athens, Greece*

(Received 4 March 1996; revised 6 November 1996)

SUMMARY

In the frame of this study, the initiation of summer storm activity over the Greek peninsula during a prevailing weak synoptic flow is investigated using the Colorado State University–Regional Atmospheric Modelling System. On 10 July 1994, thunderstorm activity was observed along a convergence zone which had developed following the main axis of the peninsula. The convergence zone first deepened the moist layer locally, providing a region potentially favourable to deep convection, while terrain variability and diurnal differential-heating-forced vertical motions. The cold air intrusion aloft, associated with the low-level convergence, resulted in deep convection and significant storm activity. The origin of the moist air masses which fed this activity has been investigated through simulations with a Lagrangian particle dispersion model. Moist air masses, which originated from marine boundary-layer of the Ionian Sea on the west, and north Aegean Sea on the east of the Greek peninsula, were transported over the land through the sea-breeze mechanism and later, at the time of the storm activity, were deeply injected into the troposphere over the convergence line, at heights up to 5 km.

KEYWORDS: Greece Lagrangian trajectories Mesoscale modelling Summer storm activity

## 1. INTRODUCTION

During summer, a regime characterized by anticyclonic subsidence, very slight barometric changes, and light winds, prevails over the Mediterranean region, due to the Azores anticyclone which develops an extension eastwards or north-eastwards. The general circulation over Europe moves toward northern latitudes and, therefore, the cyclonic activity passes north of the Alps (Meteorological Office 1962). The Greek peninsula is affected only by the edges of fronts or by upper-air troughs. This kind of synoptic-scale circulation favours the development of relatively strong thermal circulations which may trigger convergence, leading frequently to the appearance of severe weather phenomena. During early or late summer, thunderstorm activity mostly affects inland areas, while during July and August it mostly affects coastal areas (Metaxas 1972). Thunderstorm activity is less important during July and August due to the fact that the Etesian trade winds prevail over eastern Greece and the Aegean Sea. Etesian winds develop when the high pressure system over the Balkans is strong and, associated with the extension of the Anatolian-plateau thermal low, results in a strong pressure gradient over the Dardanelles and consequently in strong north-north-east winds over the Aegean Sea (Carapiperis 1951; Metaxas 1971).

Summer thunderstorm activity over Greece develops along a convergence line following the peninsula mainland axis (Metaxas 1972). Synoptic-scale lift aloft, due to cold advection at the 850/700 hPa level or potential-vorticity anomalies and/or upper-level divergence, produce an environment conducive to the development of significant convection over Greece (Solak *et al.* 1985). The degree of convection depends on the degree of instability, moisture supply and low-level convergence. The Green peninsula is characterized by complex topography and diurnal differential heating which can induce the necessary mechanical lift to transport air-masses beyond the lifting condensation level (LCL). The convergence is triggered by the thermal circulations over the area. Thermal circulations over Greece show significant spatial and temporal variations due to the significant landscape variability. As the vegetation dries out during summer the storm activity is confined to the northern part of the peninsula. This storm activity can at times be catastrophic for

* Corresponding author: University of Athens, Laboratory of Meteorology, Department of Physics, Division of Applied Physics, Bldg. PHYS-V, Panepistimioupolis, 15784 Athens, Greece.

agriculture especially over the northern part of Greece. A weather modification and hail suppression program has been in progress since 1984 at the National Agricultural Insurance Institute. During 1984–1985 and 1986, two experimental campaigns, including cloud seeding, were carried out in order to study weather modification applicability over northern Greece during summer severe weather conditions (Solak *et al.* 1985; Rudolf 1987).

Storm activity associated with enhanced convergence zones has been in evidence in the early literature since the pioneer study of Byers and Braham (1949). Studies focused on the investigation of summer storm activity in mountainous regions have illustrated the importance of daytime, thermally forced flows to local weather (Holroyd 1982; Klitch *et al.* 1985). Moreover, the convergence zones resulting from topographic conditions, surface moisture gradients and differential heating between land and water have proved to be favourable to thunderstorm activity (Pielke 1974; Schreiber 1986; Segal *et al.* 1989a, b). The influence of boundary-layer processes in initiating thunderstorms has also been investigated by Wilson *et al.* (1992).

A characteristic case of intense summer thunderstorm activity over Greece occurred on 10 July 1994. During this day, Greece was under the influence of a north-easterly synoptic flow near the surface, with cold air intrusion at 850 hPa. The 500 hPa chart revealed the presence of a trough line in the north of the Greek peninsula. Severe storm activity was observed over the peninsula at noon and in the early afternoon. In the frame of this study, the development of convergence zones and associated storm activity, as well as the origin of the warm and moist air required for such an activity, is investigated using the Colorado State University–Regional Atmospheric Modelling System (CSU–RAMS) and the Hybrid Particle and Concentration Transport Package (HYPACT). The meteorological model is used in order to investigate the mesoscale characteristics of the convergence zone developed over Greece and describe the features of the associated convective activity. The transport model is used in order to investigate the origin of the air masses feeding this activity with moisture.

In the following section the synoptic situation characterizing the case study is discussed. Section 3 is devoted to the description of the models used in this study as well as the model set-up. The model results are presented in section 4. The last section is devoted to discussion of the results and some concluding remarks.

## 2. Synoptic settings

At 0000 UTC 10 July 1994, central Europe and the Balkans were under the influence of a high pressure system associated with a very weak pressure gradient over the Greek peninsula. At 1200 UTC, the synoptic situation over the Balkans remained the same, while over the Anatolian plateau a thermal low prevailed (Fig. 1(a)). The weak pressure gradient gave rise to a weak synoptic flow in a north-easterly direction. Under these synoptic conditions local thermal circulations can develop which trigger convergence. At the 850 hPa level (Fig. 1(b)), cold-air advection is evident over the Balkans and northern Greece. Compared to the 850 hPa thermal structure of the previous day at 1200 UTC, a cooling of about 5 K was observed (not shown). At the 500 hPa level (Fig. 1(c)), there was a trough oriented from north to south with its axis extending from the eastern part of central Europe through western Greece and the Ionian Sea. This resulted in a south-westerly flow over Greece at this level. A ridge oriented north-east–south-west from the Baltic Sea through central Europe and the Iberian peninsula was also evident. The cold air advection depicted in the 850 hPa chart combined with low-level convergence resulted in convective activity over the Greek peninsula. Thunderstorms developed over northern Greece during the morning hours, then by 1200 UTC this activity affected the whole peninsula (Fig. 2). This severe

storm activity presented its maximum intensity at 1300 UTC, mainly over central Greece. Other observational evidence of the storm cells can be obtained through inspection of the satellite imagery presented in Fig. 3. Storm cells begin to develop over Albania at 0930 UTC (Fig. 3(a)). At 1230 UTC storm cells are observed over northern and central Greece and the central Peloponnese (Fig. 3(b)). Later on, the storm cells affect mainly the eastern part of the peninsula, while at 1830 UTC this activity has shifted towards the Aegean Sea and enters its decaying phase (not shown). By 2130 UTC clear sky is observed over the whole peninsula and the Aegean Sea (not shown).

In order to obtain an insight into the air mass conditions during the storm activity the rawinsonde observations from Athens (Greece), and Sofia (Bulgaria) were studied. Solak *et al.* (1985) and Rudolf *et al.* (1987), who studied severe summer weather conditions over northern Greece, concluded that the Athens sounding often provided little insight, exhibiting dry and stable conditions, while storm activity developed over northern Greece. They have proposed the sounding observations of Sofia as more representative of the air-mass characteristics associated with the summer storms. In the following, the soundings released from both the Sofia and the Athens stations are inspected. Figures 4(a) and (b) present the sounding data from Sofia at 0000 and 1200 UTC 10 July 1994, respectively. The atmosphere is moist both at night and during the day. The calculated humidity index (sum of the dew point depression at 850, 700 and 500 hPa) is 5.4 at 0000 UTC and 12.7 at 1200 UTC, showing that the atmosphere is very moist. Moreover, a cooling of the order of 4 K at 850 hPa and 2 K at 500 hPa occurs during the elapsed 12 hours, giving evidence of cold air advection aloft. At 1200 UTC the LCL is at 850 hPa while the LFC is at about 810 hPa. The instability of the atmosphere is also investigated by inspection of the wet-bulb potential temperature, $\theta_w$, profile at 0000 and 1200 UTC 10 July 1994 (Fig. 4(c)). At 0000 UTC a shallow layer of potential instability is observed close to the surface, and from 2 to 5 km, while at 1200 UTC an unstable layer ($\partial\theta_w/\partial z < 0$) is evident from the ground up to 2.5 km and from 3.5 km to 5 km. The calculated convective available potential energy (CAPE) value is 305 J kg$^{-1}$.

The skew T–log P diagram constructed from the Athens rawinsonde data at 1200 UTC 10 July 1994 is presented in Fig. 5. A cooling of the order of 3 K is observed aloft from 0000 to 1200 UTC (not shown). A shallow layer of absolute instability is observed up to 925 hPa, while the atmosphere is potentially unstable up to the 700 hPa level. Note that the atmosphere is relatively dry (especially with respect to the Sofia sounding). This may be due to the fact that the location of the sounding release is somehow far from the convergence main axis and the Athens sounding was released about one hour before the storm activity affected the area of Athens. Moreover, it is common that even in cases of strong thunderstorm activity over Athens, the sounding data do not show significant moisture loading of the atmosphere (Michalopoulou, personal communication). At 1200 UTC the LCL is at 833 hPa while the CAPE value is 2083 J kg$^{-1}$ showing that the air was potentially unstable to a high degree.

Using the ECMWF gridded analysis data at 0000 and 1200 UTC 10 July 1994, the 1000–500 hPa thickness has been calculated (Figs. 6(a) and (b)). As can be observed, a cold pool is evident over central Europe (at 0000 UTC) with cold air masses penetrating southwards over the Greek peninsula. The cold pool has moved southwards at 1200 UTC bringing colder air masses over Greece. One can also observe an intensification of the packing of the isoheight lines over Greece at 1200 UTC compared to the situation at 0000 UTC.

The synoptic settings of the atmosphere on 10 July 1994 seemed to be characteristic for the initiation of summer storm activity over the Greek peninsula. Thus, it is interesting to analyse the detailed structure of the atmosphere during this event and the characteristics and origin of the air masses which feed this storm activity, through modelling. The model

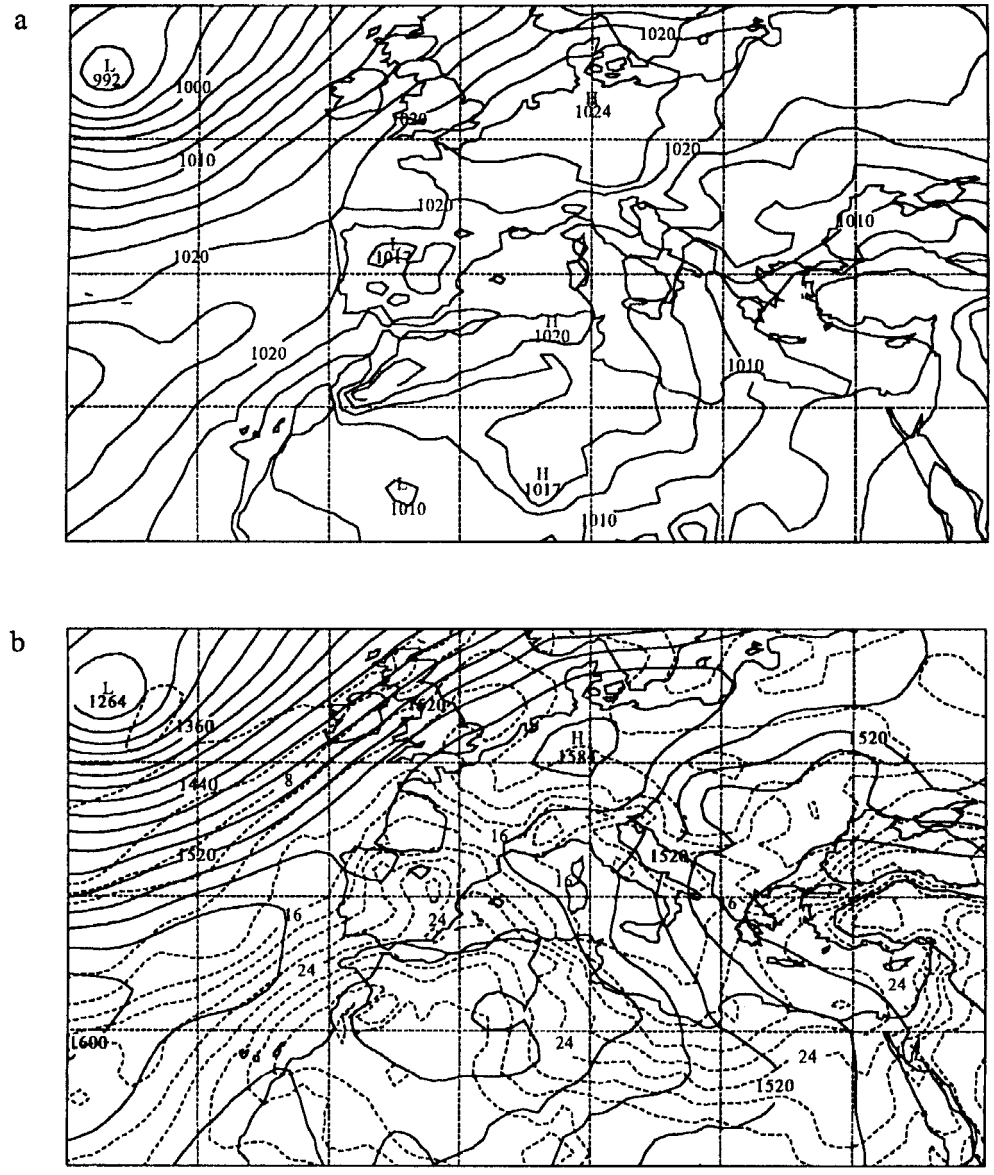


Figure 1. (a) Surface map at 1200 UTC 10 July 1994 with 2.5 hPa contour interval; (b) 850 hPa height (solid lines with 20 m interval) and temperature analysis (dashed lines with 2 deg C interval) at 1200 UTC 10 July 1994; (c) 500 hPa height (with 20 m interval) at 1200 UTC 10 July 1994.

used for this purpose and the settings used for this special study are described in the following.

## 3. Model description and set-up

### (*a*) *RAMS model*

The CSU–RAMS has been developed at the Colorado State University. It is a merger of a non-hydrostatic cloud model (Tripoli and Cotton 1982) and a hydrostatic mesoscale model (Mahrer and Pielke 1977). A general description of the model and its capacities

c

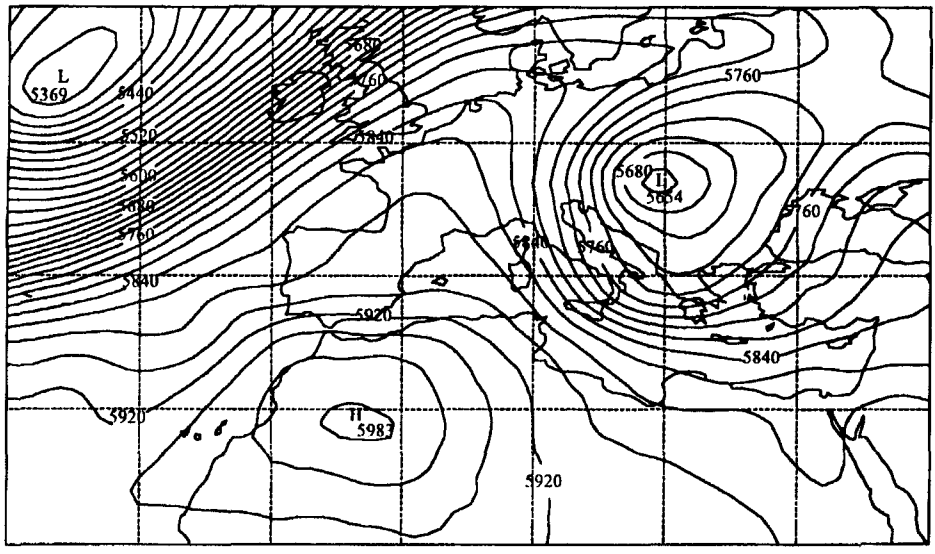


Figure 1. Continued.

is given in Pielke *et al.* (1992). However, some RAMS features are summarized in the following:

- Two-way interactive nested grid structure (Clark and Farley 1984).
- Terrain following coordinate surfaces with cartesian or polar-stereographic horizontal coordinates.
- Cloud microphysics parametrization at various levels of complexity.
- Modified Kuo cumulus parametrization (Tremback 1990).
- Radiative transfer parametrizations (shortwave and longwave) trough clear and cloudy atmospheres (Chen and Cotton 1987).
- Various options for upper and lateral boundary conditions and for finite operators.
- Various levels of complexity for surface-layer parametrization (soil-layer moisture and temperature model, vegetation parametrization etc., (see McCumber and Pielke 1981; Avissar and Mahrer 1988).

For the present application, RAMS was initialized at 0000 UTC 10 July 1994 and the duration of the simulation was 24 hours. The non-hydrostatic version of the model was employed, using two nested grids: (a) the outer, with a mesh of 64 × 68 points and 20 km horizontal grid interval centred at 39.44°N latitude and 22.5°E longitude and (b) the inner, with 98 × 118 points and 5 km horizontal grid interval, centred at 38.75°N latitude and 22.5°E longitude (Fig. 7). Thirty levels, following the topography, were used on both grids, having a 80 m vertical spacing near the ground, stretching to 1 km at 6.5 km altitude and remaining constant up to 15.5 km. Apart from these settings, a rigid lid was set at the model top boundary by constraining vertical velocity there to be zero. A soil layer has been used to predict the sensible- and latent-heat fluxes at the soil–atmosphere interface. Eleven soil levels have been used down to 50 cm below the surface. The lateral boundary conditions on the outer grid followed the Klemp–Lilly condition (Klemp and Lilly 1978) with vertical average of the gravity-wave propagation speed at the boundaries. The full

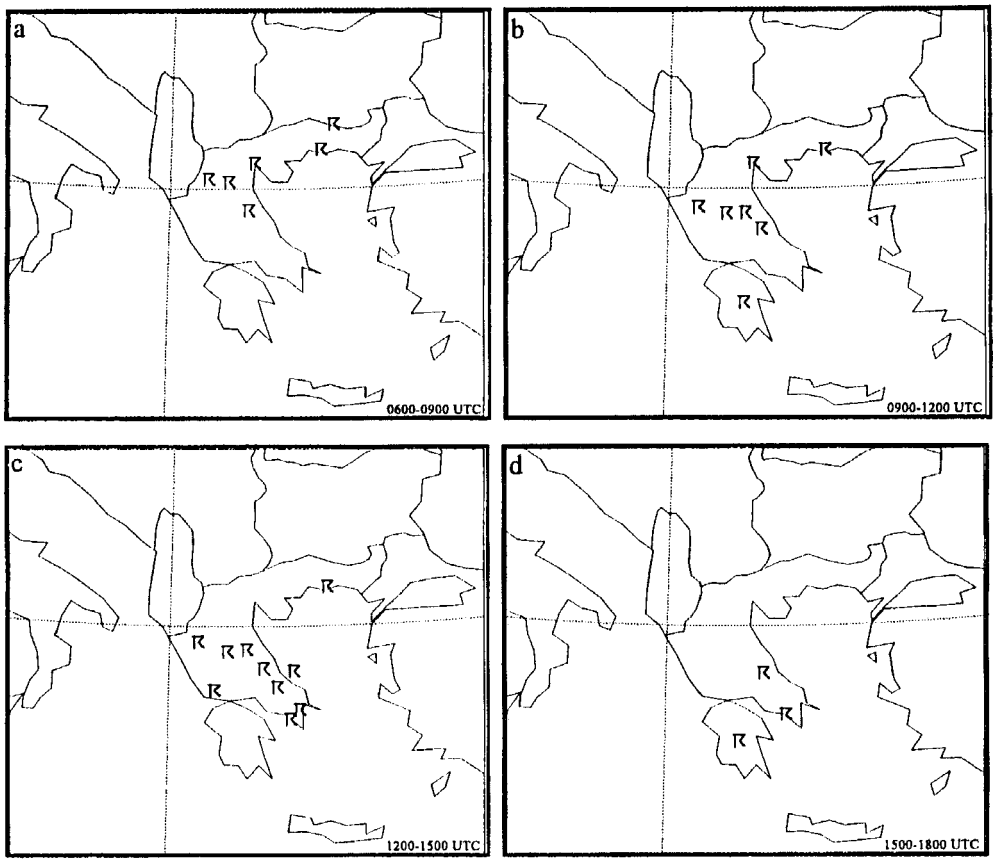


Figure 2. Reported thunderstorm activity during three-hour intervals (a) from 0600 to 0900 UTC, (b) from 0900 to 1200 UTC, (c) from 1200 to 1500 UTC and (d) from 1500 to 1800 UTC 10 July 1994.

microphysics scheme available in RAMS code was used, which activates the microphysical parametrization of rainwater, pristine ice, snow, graupel and aggregates. In addition, the cumulus parametrization options in RAMS were employed.

The ECMWF 1° gridded analysis fields were used in order to initialize the model. The ECMWF data are objectively analysed by the RAMS model on isentropic surfaces, from which they are interpolated to the RAMS grids. These fields were used in order to nudge the lateral boundary region of the coarser grid every six hours. Climatological sea-surface temperature of 1° spatial resolution retrieved by NCAR and topography derived from 30″ resolution terrain data were used for both grids. Finally, gridded vegetation-type data of 10′ resolution were used.

### (*b*) *The HYPACT model*

The HYPACT model has been developed at the Colorado State University and ASTER Division of Mission Research Corporation. As described in Tremback *et al.* (1994), the model consists of a combination of a Lagrangian particle model and an Eulerian concentration–transport model. The Lagrangian model handles the subgrid-scale aspects of particle release while the Eulerian model takes over when the particle 'cloud' becomes adequately resolved on the computational grid, thus reducing the number of particles needed and increasing the computational efficiency. Its two-way interactive nesting (like

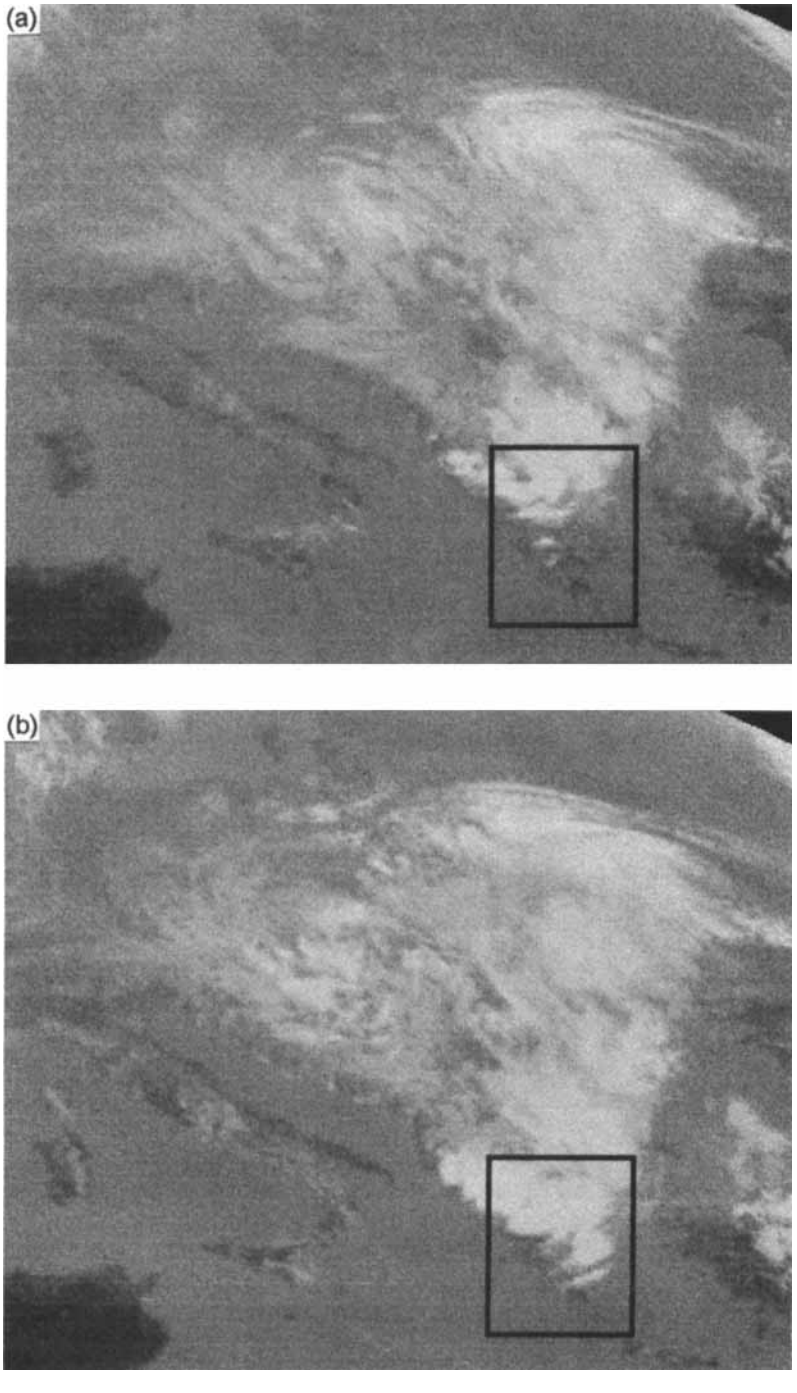


Figure 3. METEOSAT infra-red pictures at (a) 0930 UTC and (b) 1230 UTC 10 July 1994. The rectangle denotes the approximate position of the inner grid of RAMS simulations (photos European Space Agency–ESA).

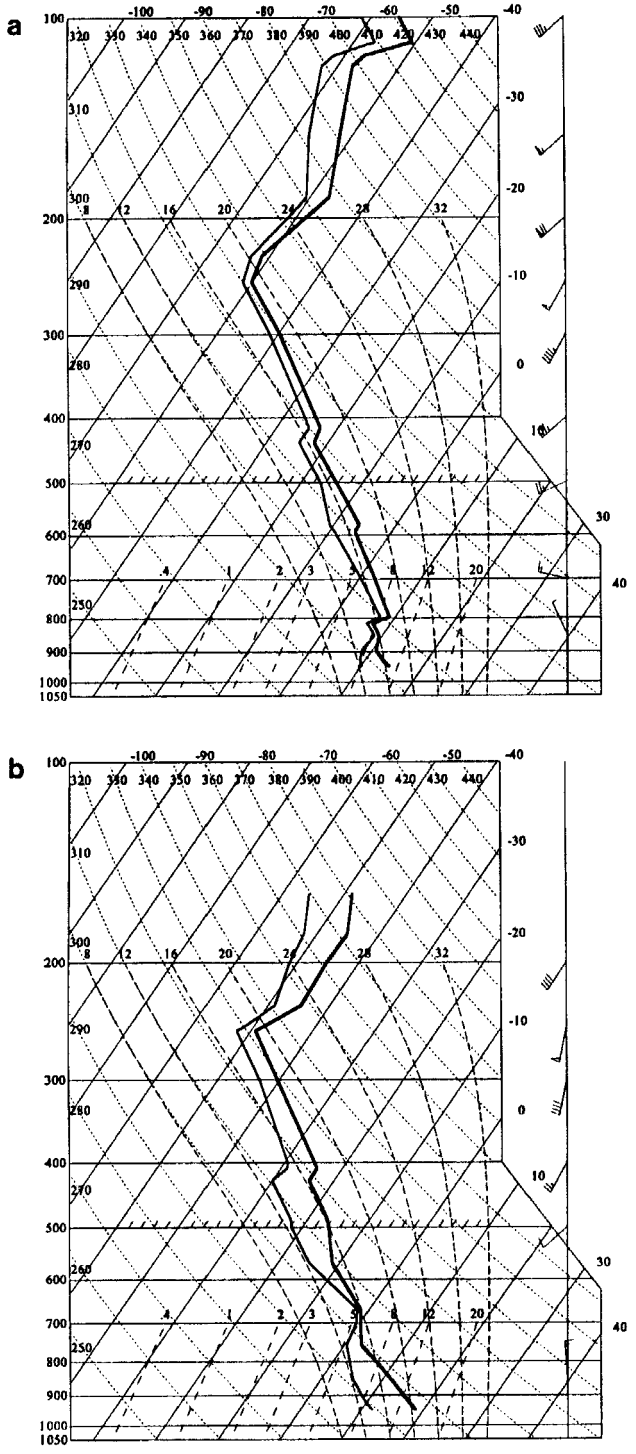


Figure 4. Skew T–log P diagram constructed from the sounding released from Sofia (Bulgaria) at (a) 0000 UTC and (b) 1200 UTC 10 July 1994. One pennant equals 25 m $s^{-1}$, one full barb equals 5 m $s^{-1}$ and one half barb equals 2.5 m $s^{-1}$. (c) vertical profile of wet-bulb potential temperature at 0000 UTC (rectangles) and at 1200 UTC (open circles).

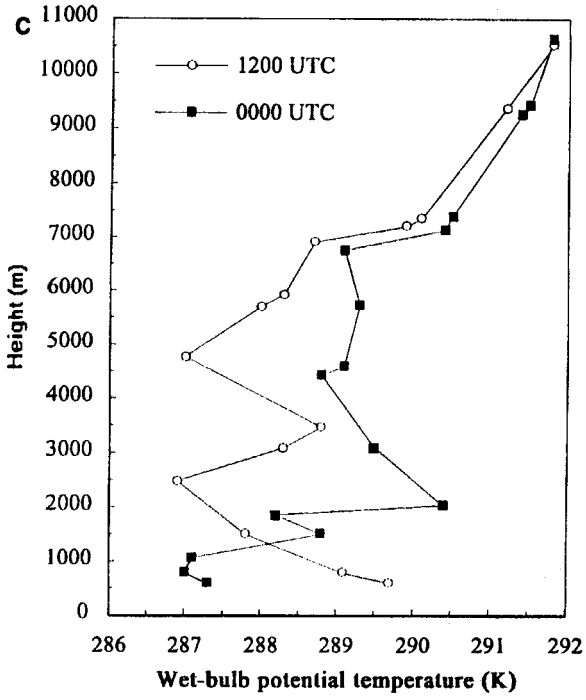


Figure 4. Continued.

RAMS) permits the transport of air particles across the domains. This feature eliminates boundary value problems which might be important in cases of small domains. The HYPACT Lagrangian model uses the velocity and turbulence fields simulated by RAMS in order to advect the particles with mean and random turbulent wind components. HYPACT uses a level-2.5 turbulent closure scheme based on the prognostic turbulent kinetic energy from RAMS. HYPACT was used instead of trajectory calculations because it includes all the turbulent properties of the flow which are quite important in mesoscale thermal circulations.

For the present application, HYPACT was initialized at 0000 UTC 10 July 1994, and the duration of the simulation was 24 hours. The Lagrangian version of the model was used. In order to study the origin of the air masses feeding the convergence zone over the Greek peninsula, an area of hypothetical moist air parcels was defined within the marine boundary-layer over the Ionian Sea to the west of the peninsula and over the northern Aegean Sea to the east of the peninsula. The areas were selected following the flow patterns simulated by RAMS.

## 4. Model results

The wind field, at $z = 225$ m AGL, in the outer grid of RAMS is presented in Fig. 8. At 0600 UTC north-north-westerly winds are evident over the Ionian Sea, backing to a north-westerly direction in the region south of the Peloponnese. A north-easterly flow is evident over north-eastern Greece and the Caspian Sea, backing to northerly and then north-westerly directions at the exit of the Aegean Sea. The flow is intensified in the region north-east of Crete (Fig. 8(a)). The flow over the Aegean Sea is consistent with the synoptic pattern presented in Fig. 1(a). The consistency of the model results can be

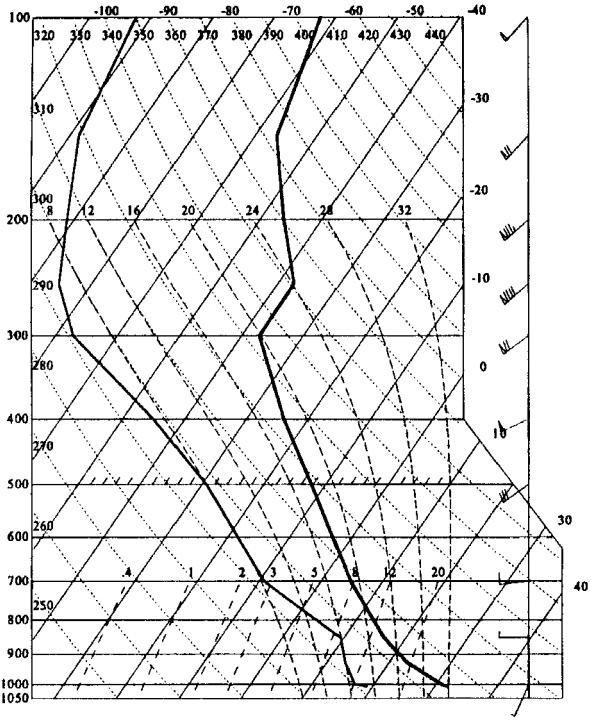

Figure 5. Skew T–log P diagram constructed from the sounding released from Athens at 1200 UTC 10 July 1994. One pennant equals 25 m $s^{-1}$, one full barb equals 5 m $s^{-1}$ and one half barb equals 2.5 m $s^{-1}$.

confirmed through inspection of the winds provided from the surface synoptic network (Fig. 8(b)). The comparison between the observed and predicted fields shows a good agreement, with north-westerly winds over the Ionian Sea and north-easterly winds over the Aegean Sea. As discussed in section 2, the prevailing synoptic situation favours the development of local thermal circulations. These circulations begin to develop at 1000 UTC and are intensified in the following hours. The wind pattern at 1300 UTC is presented in Fig. 8(c). Over the Greek peninsula, organized convergence is evident on an axis oriented north-west to south-east through central Greece, following the main axis of the topographic ridge (Fig. 7(b)). Convergence over the southern part of the peninsula is also evident. Note also the backing of the wind over the eastern Aegean Sea compared to the 0600 UTC wind pattern and the inflow toward the western coast of Turkey. The predicted fields are in good agreement with the winds reported at 1200 UTC by the surface synoptic network (Fig. 8(d)). The organized convergence along the main axis of the peninsula gives rise to a mechanical lifting of the air masses which meet a colder layer aloft. The cold air advection at 700 and 500 hPa is evident through inspection of the temperature fields derived by RAMS at 0000 UTC and 1200 UTC (Fig. 9). Note the position of the 4 °C isotherm which is shifted within 12 hours from the region of Albania to northern Greece at the 700 hPa level (Figs. 9(a) and (b)), as well as the shift of the −14 °C isotherm from the area over Albania towards central Greece at the 500 hPa level (Figs. 9(c) and (d)).

Differential heating and complex topography give rise to quite strong vertical motions over the Greek peninsula. At 0600 UTC the updrafts at z = 1500 m AGL did not exceed 0.4 m $s^{-1}$ (not shown). Significant ascending motions begin to develop at 0900 UTC, reaching the maximum horizontal extensions and best organization from 1200 to 1400 UTC. Figure 10 presents a horizontal cross-section of the vertical velocity field, inside the inner

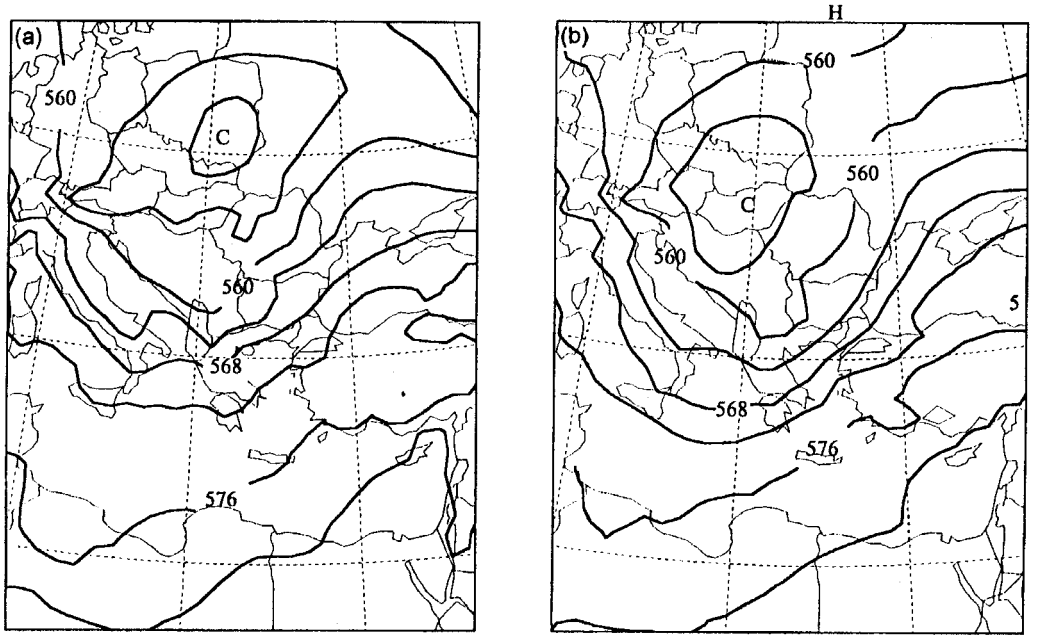


Figure 6. 10000–500 hPa thickness at (a) 0000 UTC and (b) 1200 UTC 10 July 1994 at 4 dm intervals.

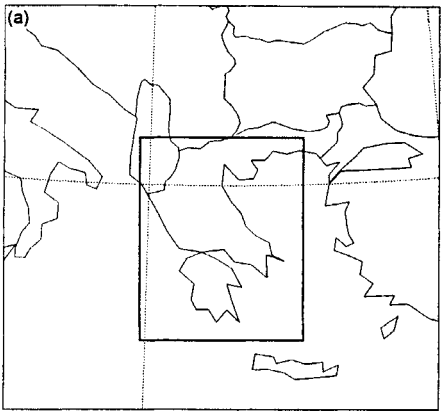


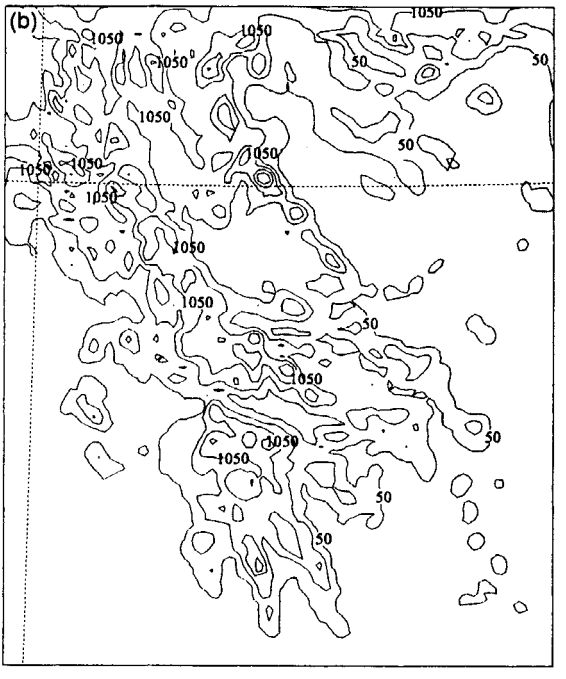


Figure 7. (a) Domain of the two nested grids of RAMS. (b) Representation of the inner grid topography, contoured every 500 m.

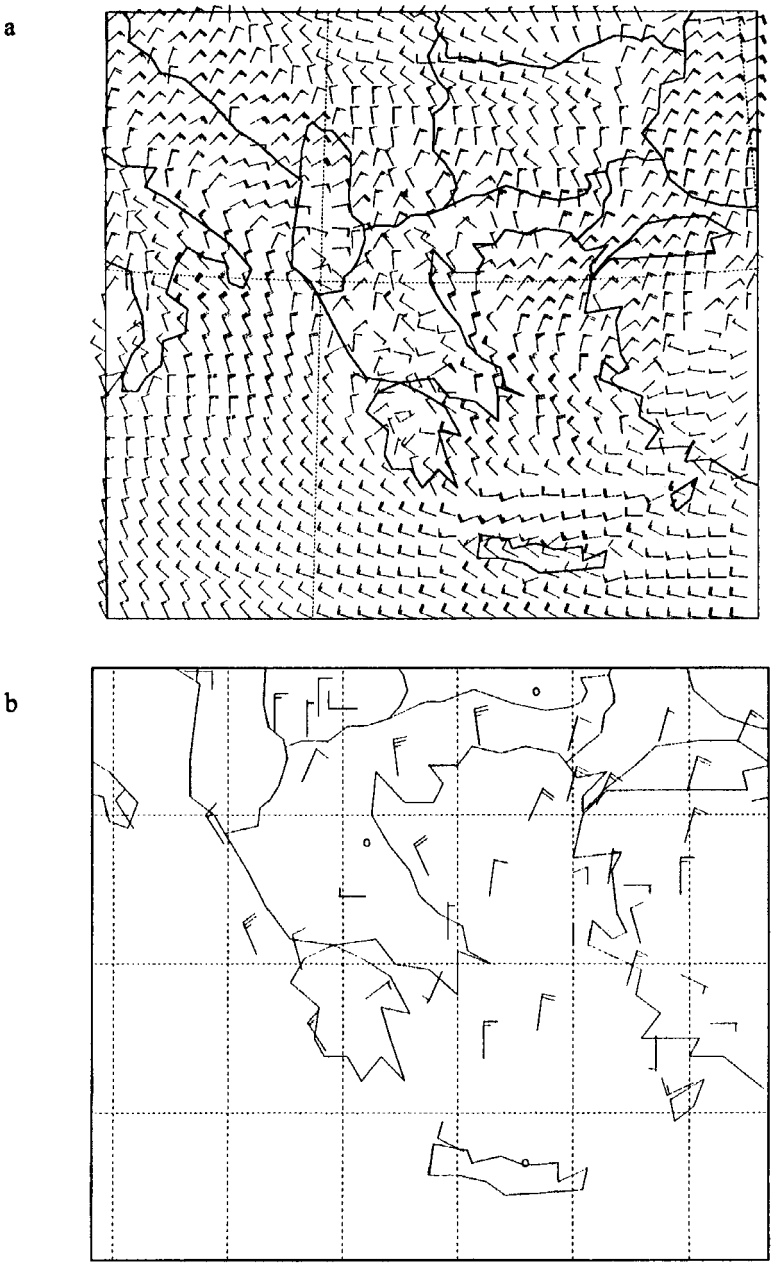


Figure 8. (a) Horizontal cross-section of RAMS outer grid at z = 225 m AGL at 0600 UTC 10 July 1994. (b) Observed winds from the surface synoptic network at 0600 UTC. (c) As in (a), but at 1300 UTC, and (d) as in (b), but at 1200 UTC. Wind symbols are plotted every second grid-point in (a) and (c). One pennant equals 20 m $s^{-1}$, one barb 4 m $s^{-1}$ and one half barb 2 m $s^{-1}$.

c

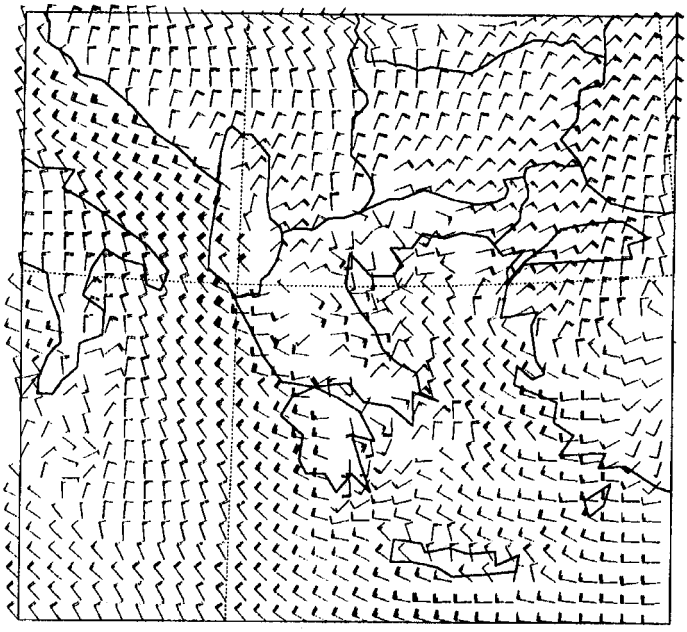

d

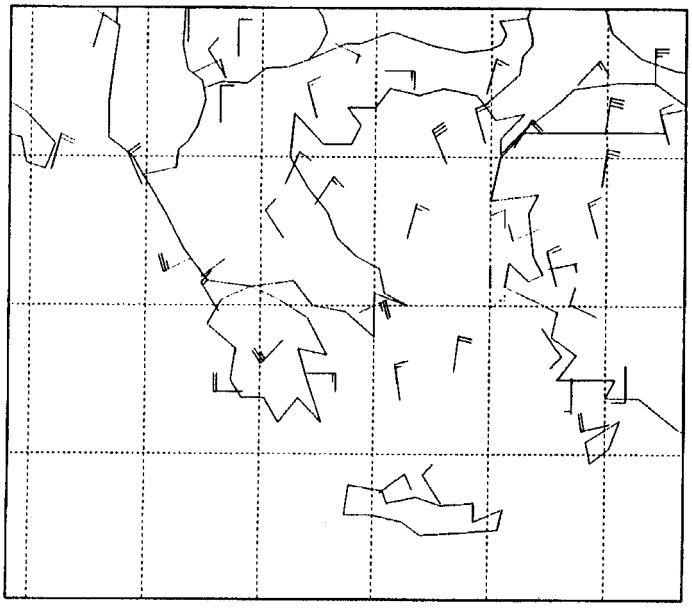

Figure 8. Continued.

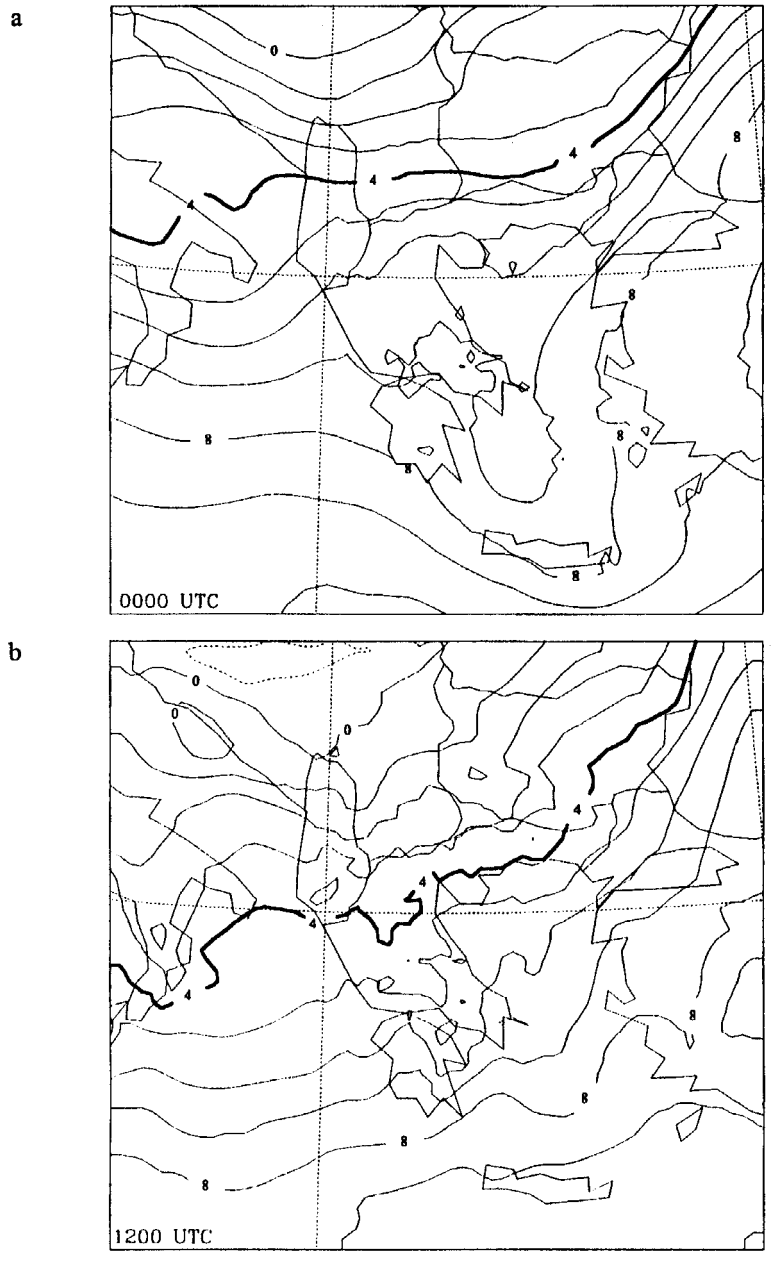


Figure 9. Horizontal cross-section of the temperature field of RAMS outer grid at the 700 hPa isobaric level at (a) 0000 UTC, (b) 1200 UTC 10 July 1994. (c) As in (a), but at 500 hPa and (d) as in (b), but at 500 hPa. Dashed lines indicate negative temperatures. Contours are at 1 deg C interval.

c

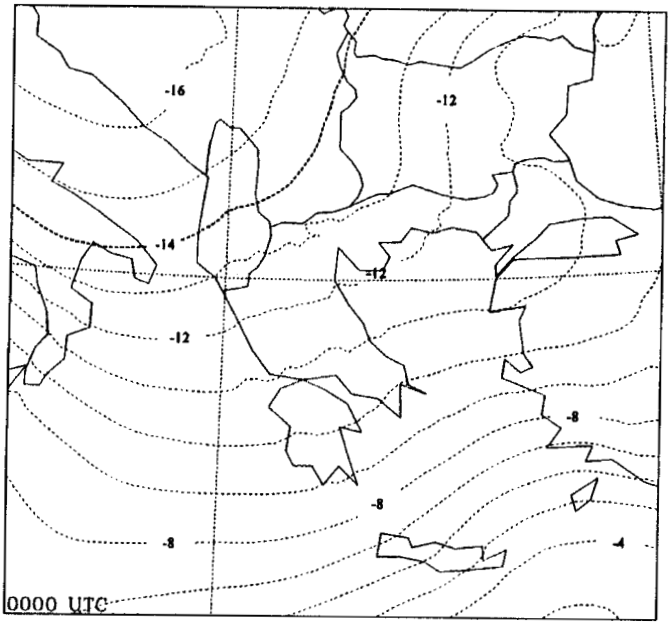


d

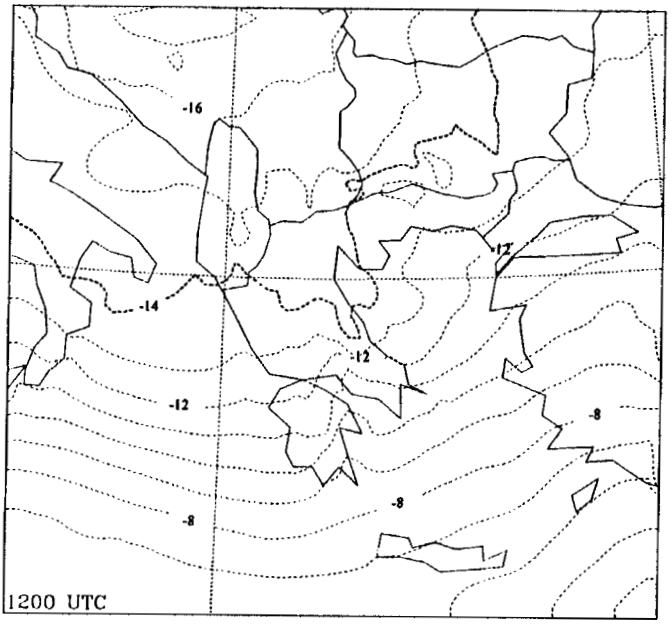


Figure 9. Continued.

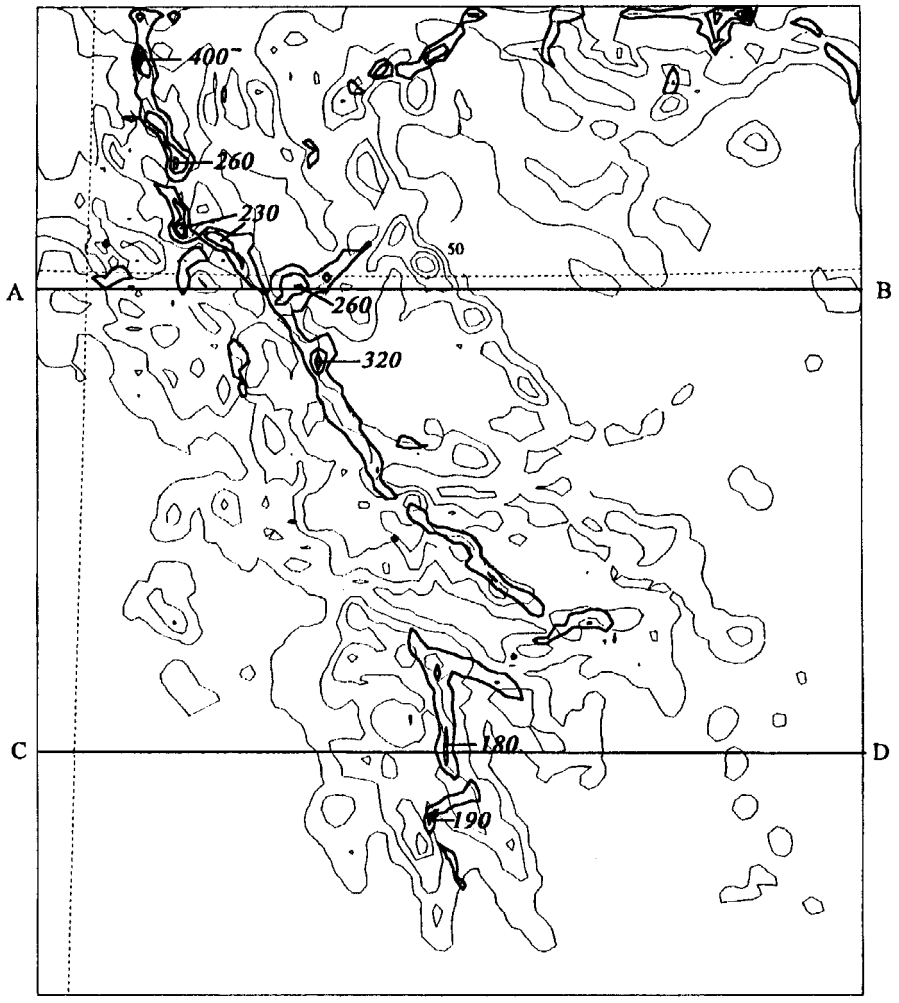


Figure 10. Horizontal cross-section of RAMS inner grid at z = 1500 m AGL at 1300 UTC 10 July 1994. Bold lines denote vertical velocity with 100 cm $s^{-1}$ interval. Only values exceeding 50 cm $s^{-1}$ are shown, while maximum values at each location are denoted with bold numbers (in cm $s^{-1}$). Topography is contoured every 500 m. Line CD indicates the location of the vertical cross-sections given in Fig. 11 and line AB the location of cross-sections given in Fig. 12.

grid of RAMS, at $z = 1500$ m AGL at 1300 UTC. A band of significant upward vertical motion is evident following the convergence zone depicted in Fig. 8(b). The strongest updrafts are evident over central Greece and Albania, exceeding 3.5 m $s^{-1}$. Inspection of the vertical velocity horizontal cross-sections at higher levels (not shown) revealed that the deepest convective motions occur over northern Greece, while the updrafts developed over the southern part of the peninsula are relatively shallow, not exceeding 3 km in altitude.

In order to assess an image of the vertical structure of atmosphere during this event vertical cross-sections of parameters indicative of the strength of convection, such as vertical velocity, turbulent kinetic energy (TKE), and mixing ratio have been constructed. Figure 11(a) presents the vertical velocity field at 1300 UTC in a cross-section over southern Greece. Updrafts are evident on the eastern side of the mountains, but they are relatively shallow. Convection does not exceed 3 km in height with a maximum of about 2 m $s^{-1}$ at

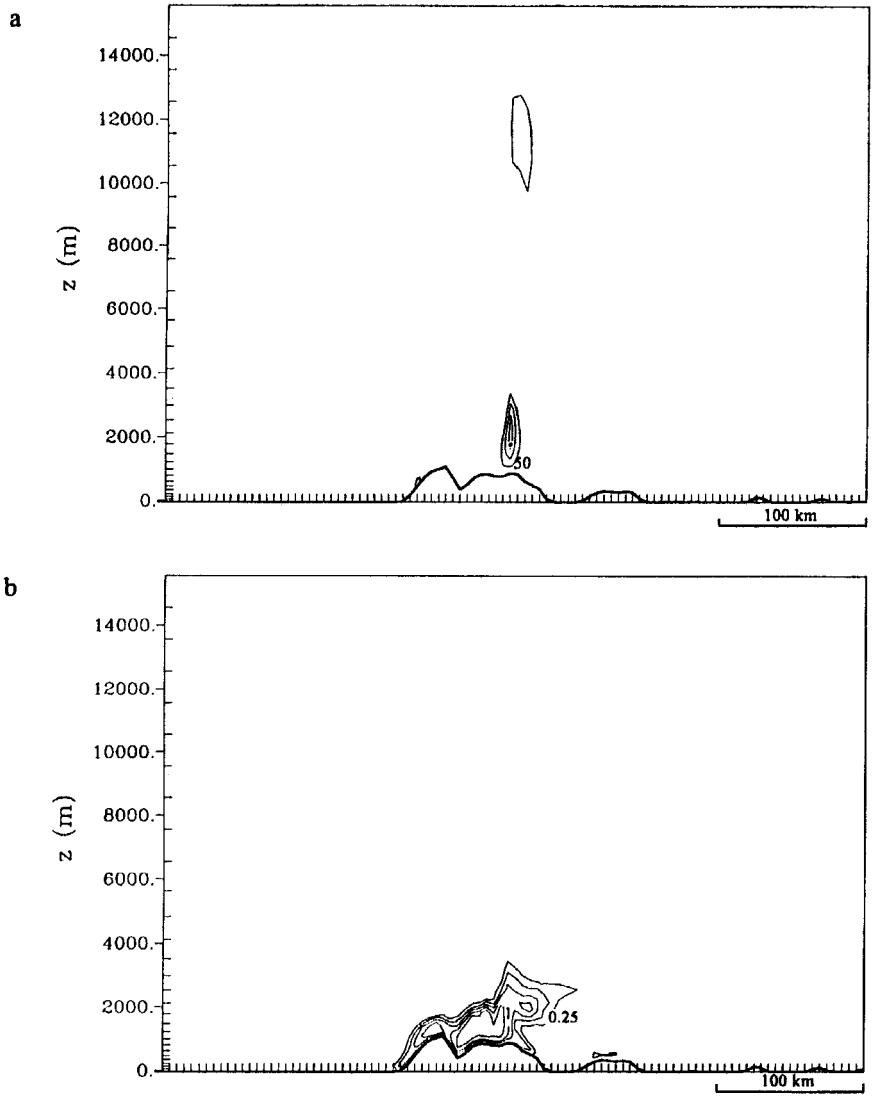


Figure 11. Vertical cross-sections of RAMS inner grid following the line CD on Fig. 10 at 1300 UTC 10 July 1994, of (a) vertical velocity (with 50 cm $s^{-1}$ interval, only values exceeding 50 cm $s^{-1}$ are shown) and (b) turbulent kinetic energy (with 0.25 $m^2$ $s^{-2}$ interval).

about z = 2 km. The TKE pattern (Fig. 11(b)) shows a maximum of 1.4 $m^2$ $s^{-2}$ confined to the lowest 1.5 km.

Convection is significantly deeper over the central part of Greece. At the time of the initiation of thunderstorm activity at 1000 UTC updrafts with a maximum of 2 m $s^{-1}$ (confined to the first 4 km) are observed in the western part of the peninsula (Fig. 12(a)). Later on, at the time of maximum activity (1300 UTC), the updrafts extend up to z = 10 km with a maximum of 5 m $s^{-1}$ at about z = 6 km (Fig. 12(c)). The convective cells are now shifted about 100 km towards the east, in agreement with the position of the convective cells depicted in the satellite image (Fig. 3) and the regions of observed significant thunderstorm activity (Fig. 2). Inspection of the vertical cross-sections of total mixing ratio at 1000 and

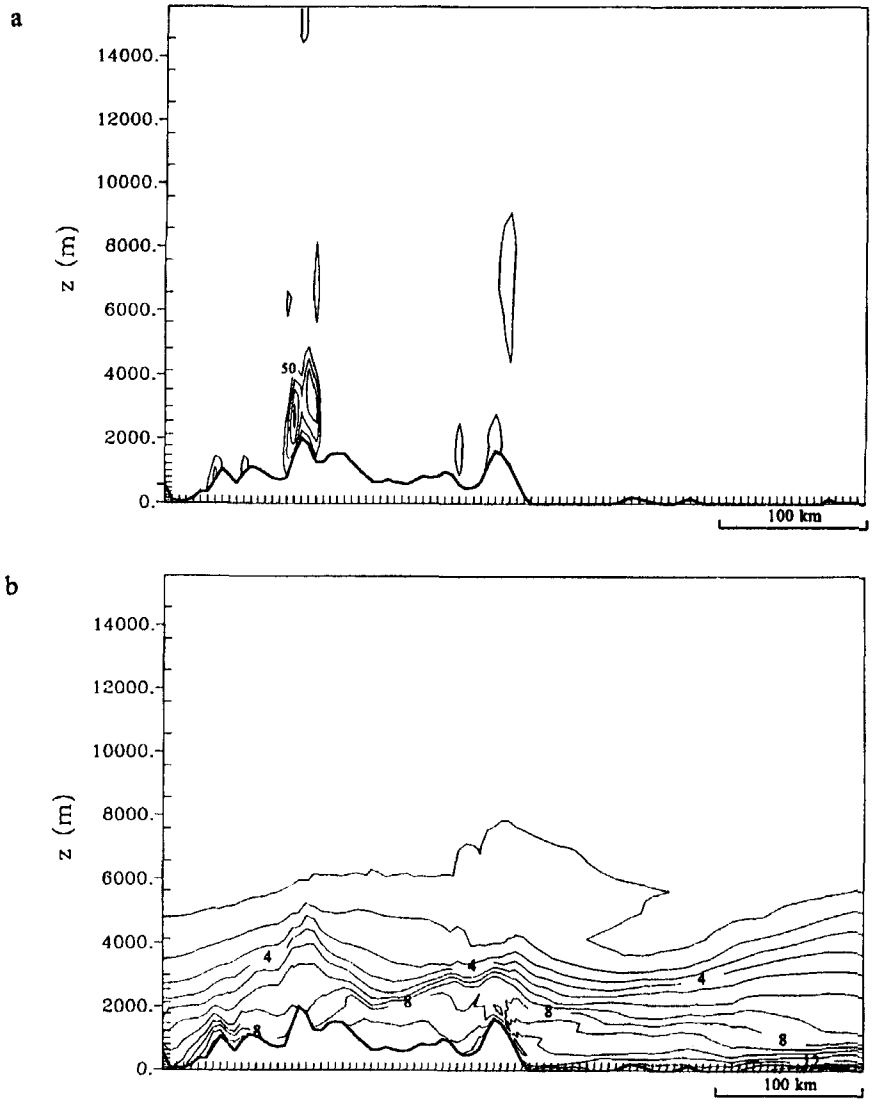


Figure 12. Vertical cross sections of RAMS inner grid following the line AB on Fig. 10 of (a) vertical velocity (at 50 cm $s^{-1}$ interval, only values exceeding 50 cm $s^{-1}$ are shown) at 1000 UTC and (b) total mixing ratio (at 1 g $kg^{-1}$ interval) at 1000 UTC. (c) As in (a), but at 1300 UTC, and (d) as in (b), but at 1300 UTC. (e) West–east wind component (with 5 m $s^{-1}$ interval, negative values indicating eastern flow are dashed) at 1300 UTC and (f) turbulent kinetic energy (with 0.25 $m^2$ $s^{-2}$ interval) at 1300 UTC.

1300 UTC (Figs. 12(b) and (d), respectively) reveals the inflow of moist air masses from the maritime regions on both sides of the peninsula which feed the convective activity and are injected aloft in the region of maximum convection. Note the position of the 4 g $kg^{-1}$ isoline which is injected from an altitude of 2.5 km to about 4 km within 3 hours (from 1000 to 1300 UTC). The convergence of air masses over the area is also depicted in the $u$-component wind field (Fig. 12(e)). Moist air masses of more than 8 g $kg^{-1}$ are advected from the eastern flow prevailing in the first 2 km above the sea towards the land. The TKE pattern gives a maximum of 2 $m^2$ $s^{-2}$ (Fig. 12(f)) in the region of maximum convective activity while the isoline of 0.5 $m^2$ $s^{-2}$ extends up to about 5 km.

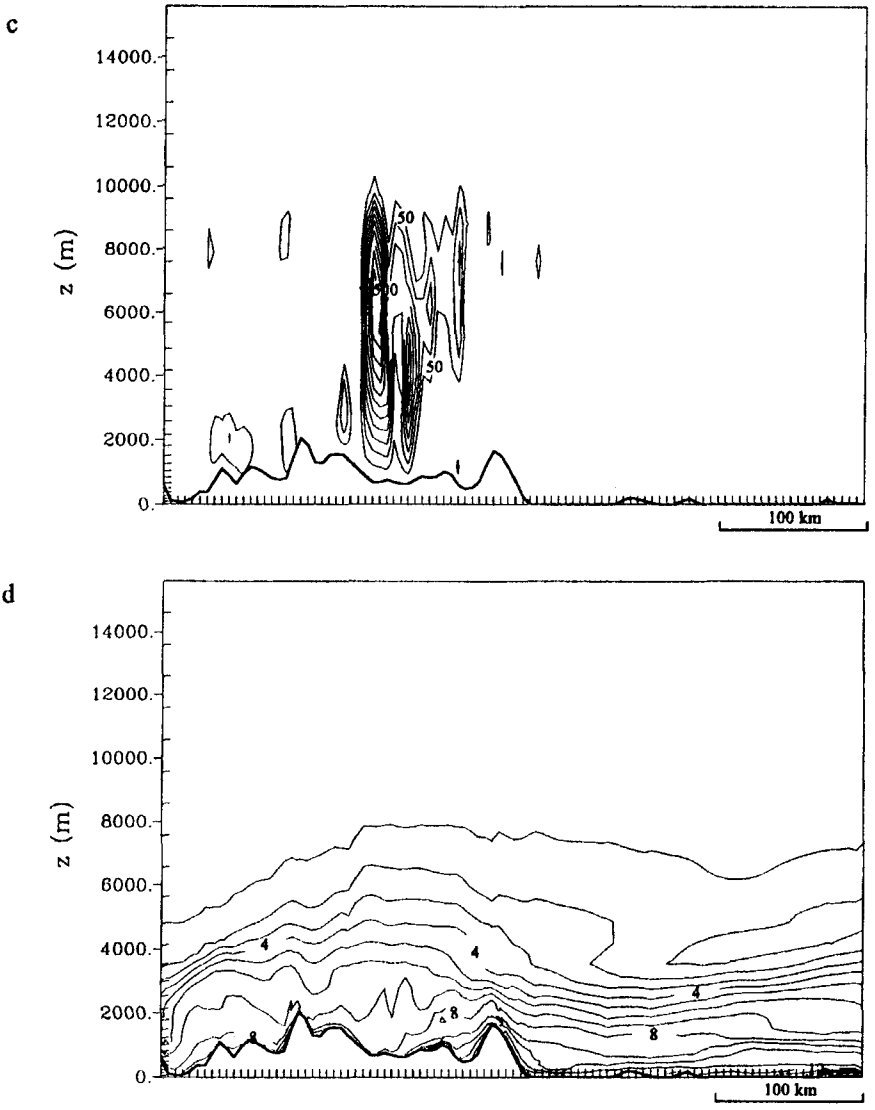


Figure 12. Continued.

Inspection of the meteorological fields predicted by RAMS suggested that the convective activity was sustained by the inflow of wet air masses from both the Ionian Sea to the west and the Aegean Sea to the east of the peninsula. The origin of the air masses feeding the convective activity with moisture was studied using the HYPACT dispersion model. Particle releases were used as tracers of air masses originating from the marine boundary-layer. The use of a Lagrangian particle model presents several advantages compared to the derivation of simple trajectories. The main advantage is the follow-up of the motion of the whole spectrum represented by the model plus turbulence.

Two areas of hypothetical particle release, following a belt parallel to the coast, were defined within the marine boundary-layer (within the first 250 m) of (a) the Ionian Sea and (b) the northern Aegean Sea. The position of the sources, as well as the distance from

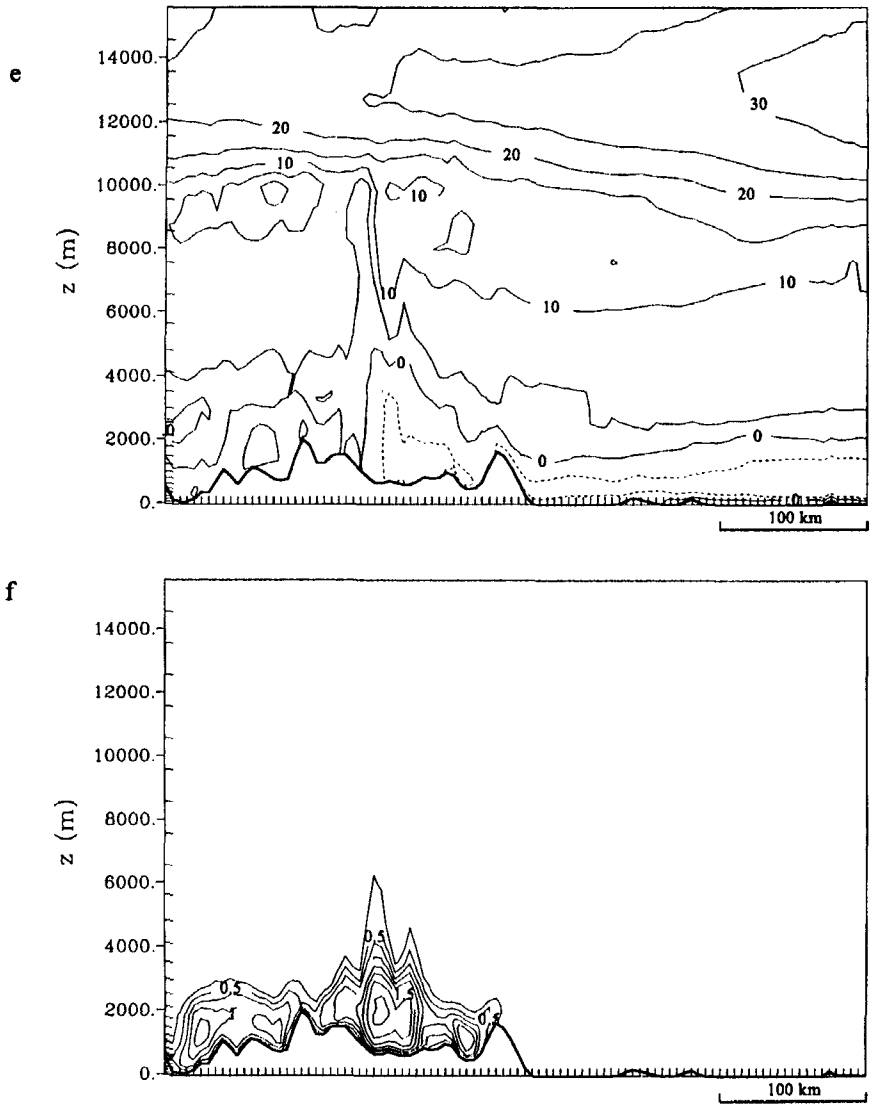


Figure 12. Continued.

the coast, was defined based on the inspection of the wind flow presented in Fig. 8. The release of particles started at 0000 UTC 10 July 1995 and was continuous during the whole simulated period (24 hours).

Figure 13(a) presents the position of the hypothetical particles at 1400 UTC, after 14 hours of continuous release. During the morning hours, the air masses are advected by the synoptic flow southwards, away from the peninsula, while later on the development of local thermal circulations begins to advect the air masses towards the coasts of Greece. These air masses enter within the mainland and at 1400 UTC they converge towards the main mountain axis. A vertical cross-section within the region of maximum ascending motions (Fig. 13(b)) demonstrates the injection of the moist air masses inside the updraft region. Released particles enter the region of upward motions and they are found up to 4 km.

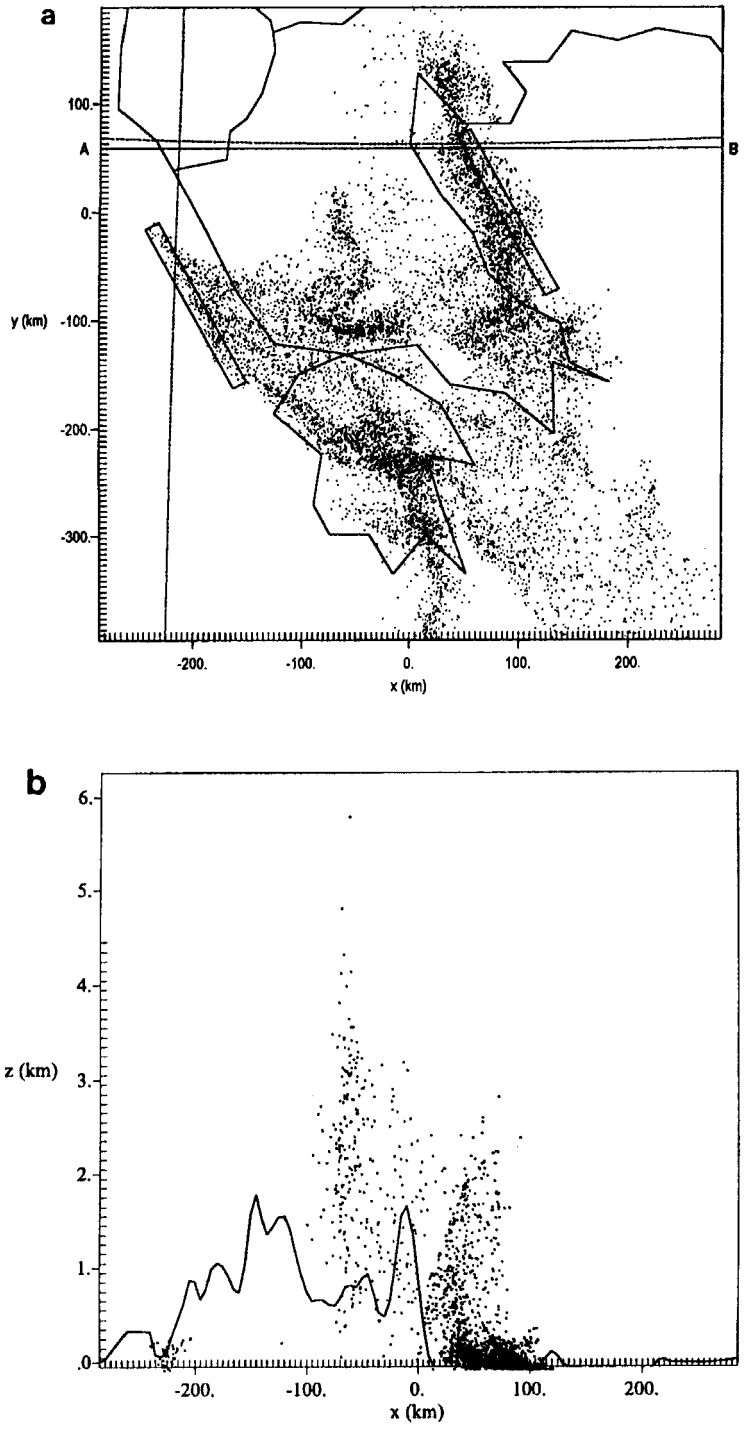


Figure 13. (a) Hypothetical moist particles position at 1400 UTC 10 July 1994. Rectangles indicate the position of the hypothetical area source of moist particles. Line AB gives the location of the vertical cross-section presented in (b). (b) Position of hypothetical moist particles, in a vertical cross-section following the line AB in (a).

## 5. Discussion and concluding remarks

In the frame of this paper, a typical summer storm activity occurring over Greece has been investigated. This event was characterized by a weak synoptic flow which favours the development of local thermal circulations. Under these synoptic conditions a convergence zone develops over Greece. This convergence zone is often observed during summer, except when the Etesian trade winds prevail. The convergence and the associated ascending motions are confined within the first 3 km and they are not sufficient to trigger deep convection and thunderstorm activity unless cold air advection at the lower and middle tropospheric layers (within the 850–500 hPa layer) occurs.

The 10 July 1994 event was characterized by a cold advection in the layer from 850 to 500 hPa as depicted by the synoptic charts and the sounding data of nearby stations and predicted by the model. Under the prevailing weak synoptic conditions, the developed convergence associated with the cold advection aloft triggered deep convection and thunderstorm activity over the Greek peninsula. The event has been simulated using the RAMS meteorological model and the HYPACT transport model. RAMS performed a rather realistic simulation of this storm activity, while the transport model revealed the origin of the air masses which fed the storm with moisture. The analysis of model results suggested the following:

- The intrusion of cold air within the lower tropospheric layers was reproduced over central and northern Greece. A cooling of about 2.5 K at the 700 hPa level, and 2 K at the 500 hPa, was evident from 0000 UTC to 1200 UTC.
- Convergence zones began to form over northern Greece at 1000 UTC and three hours later were evident over the main axis of the peninsula.
- The strongest updraft motions were observed over the main axis of the Greek peninsula and especially over areas with significant topographic features. These updrafts extend up to about 8 km height.
- Dispersion simulations suggested that the necessary moisture for the heavy precipitation in northern and central Greece was provided by the marine boundary-layer of the northern Aegean Sea. Inspection of vertical cross-sections over northern Greece revealed that the moist air masses originated from the northern Aegean Sea, were injected up to 5 km, and that they were confined to the eastern part of the orographic axis. Moist air masses from the Ionian Sea fed the southern part of the Greek peninsula with moisture.
- The thunderstorm activity showed a selective spatial distribution due to the locality of thermal circulations.

This last point needs to be discussed more extensively. Thunderstorm activity was more pronounced over northern Greece where the deepest convective vertical motions occurred. This can be attributed to the fact that cooling at the lower and mid tropospheric layers was more pronounced over northern Greece. Moreover, the selective spatial distribution of the observed thunderstorm activity could be correlated with the more vegetated and irrigated areas which supply the convective cells with moisture. Indeed, the impact of vegetation and soil wetness on the moisture within the boundary layer and the potential for development of convective clouds has been pointed out by Segal *et al.* (1989a, b). Recently these effects have been summarized in Ramamurthy (1995). The study of the role of surface properties on the spatial and temporal distribution of thunderstorm activity over Greece deserves further investigation. This modelling study could be performed when vegetation type data of high spatial resolution and for different periods of the year, as well as information about soil moisture and extension of irrigated areas, is available.

## ACKNOWLEDGEMENTS

This research was partially supported by the AVICENNE Initiative, contract number EV*-CT92-0005 of the DG-XII of the Commission of the European Communities. The authors are grateful to Dr. C. Tremback (Aster Division of Mission Research Corporation) for his helpful suggestions on the model settings and to Professors V. Notaridou and D. Pisimanis for fruitful discussions. Ms M. Varinou and Mr S. Dobricic are also kindly acknowledged. Acknowledgement is made to the National Center for Atmospheric Research, which is sponsored by the National Science Foundation, for some of the computing time used in this research, and for providing the sounding and surface data used in this study (Contract #35081147).

## REFERENCES

Avissar, R. and Mahrer, Y. 1988 Mapping frost sensitive areas with a three dimensional local scale numerical model. Part I: Physical and numerical aspects. *J. Appl. Meteorol.*, **27,** 400–413

Byers, H. R. and Braham, R. R. 1949 *The Thunderstorm.* U.S. Government Printing Office, Washington, D.C., 287

Carapiperis, L. N. 1951 On the periodicity of the Etesian in Athens. *Weather*, **6,** 378–380

Chen, C. and Cotton, W. R. 1987 The physics of the marine stratocumulus-capped mixed layer. *Boundary-Layer Meteorol.*, **25,** 289–321

Clark, T. L. and Farley, R. D. 1984 Severe downslope windstorm calculations in two and three spatial dimensions using anelastic interactive grid nesting: A possible mechanism for gustiness. *J. Atmos. Sci.*, **41,** 329–350

Holroyd, E. W. 1982 Some observations on mountain-generated cumulonimbus rainfall on the northern Great Plains. *J. Appl. Meteorol.*, **21,** 560–565

Klemp, J. B. and Lilly, D. K. 1978 Numerical simulation of hydrostatic mountain waves. *J. Atmos. Sci.*, **35,** 78–107

Klitch, M. A., Weaver, J. F., Kelly, F. P. and VonderHaar, T. H. 1985 Convective cloud climatologies constructed from satellite imagery. *Mon. Weather Rev.*, **113,** 326–337

Mahrer, Y. and Pielke, R. A. 1977 A numerical study of the airflow over irregular terrain. *Beit. Phys. Atmos.*, **50,** 98–113

McCumber, M. C. and Pielke, R. A. 1981 Simulation of the effects of surface fluxes of heat and moisture in a mesoscale numerical model. Part I: Soil layer. *J. Geophys. Res.*, **86,** 9929–9938

Metaxas 1971 'The Etesians. Digest of selected weather problems of the Mediterranean'. Navy Weather Research Facility, 127

1972 'Space and distribution of thunderstorm frequency in Greece'. Publications of the Laboratory of Meteorology, University of Ioannina, Greece (in Greek, extended abstract in English)

Meteorological Office 1962 Weather in the Mediterranean. *Vol. I, General Meteorology.* H.M.S.O., London. Second Edition

Pielke, R. A. 1974 A three-dimensional numerical model of the sea breezes over South Florida. *Mon. Weather Rev.*, **102,** 115–139

Pielke, R. A., Cotton, W. R., Walko, R. L., Tremback, C. J., Lyons, W. A., Grasso, L. D., Nicholls, M. E., Moran, M. D., Wesley, D. A., Lee, T. J. and Copeland, J. H. 1992 A comprehensive meteorological modelling system–RAMS. *Meteorol. Atmos. Phys.*, **49,** 69–91

Ramamurthy, M. K. 1995 The 10th AMS conference on numerical weather prediction, Portland, Oregon, 18–22 July 1994. *Bull. Amer. Meteorol. Soc.*, **76,** 2211–2240

Rudolf, R. C., Davis, A. G., Dalezios, N. R. and Tanton, S. C. 1987 'The 1986 Greek National Hail Suppression Program'. Annual Report. Available at the National Agricultural Insurance Institute, 30 Patission Str., Athens, Greece

Schreiber, W. E. 1986 Case studies of thunderstorm initiated by radar-observed convergence lines. *Mon. Weather Rev.*, **114,** 2256–2266

Segal, M., Schreiber, W. E., Kallos, G., Garratt, J. R., Rodi, A., Weaver, J. and Pielke, R. A. 1989a The impact of crop areas in Northeast Colorado on midsummer mesoscale thermal circulations. *Mon. Weather Rev.*, **117,** 809–824

Segal, M., Garratt, J. R., Kallos, G. and Pielke, R. A. 1989b On the impact of wet soil and canopy temperatures on daytime boundary-layer growth. *J. Atmos. Sci.*, **46,** 3673–3644

Solak, M. E., Melita, D. C., Allan, R. B., Henderson, T. J., Duckering, D. W. and Pinion, S. D. 1985 'The 1984–1985 National Hail Suppression Program in Greece'. Available at the National Agricultural Insurance Institute, 30 Patission Str., Athens, Greece

Tremback, C. J. 1990 'Numerical simulation of a mesoscale convective complex: Model development and numerical results'. Ph.D. dissertation, Atmos. Sci. Paper No. 465, Colorado State University, Dept. of Atmos. Science, Fort Collins, Co 8523

Tremback, C. J., Lyons, W. A., Thorson, W. P. and Walko, R. L. 1994 An emergency response and local weather forecasting software system. Pp. 423–429 in Proc. of the 20th ITM of NATO/CCMS on Air Pollution Modelling and its Application. Eds. S. Gryning and M. Millan. Plenum Press

Tripoli, G. J. and Cotton, W. R. 1982 The Colorado State University three-dimensional cloud/mesoscale model–1982. Part I: General theoretical framework and sensitivity experiment. *J. Rech. Atmos.*, **16,** 185–220

Wilson, J. W., Foote, G. B., Crook, N. A., Fankhauser, J. C., Wade, C. G., Tuttle, J. D. and Mueller, C. K. 1992 The role of boundary-layer convergence zones and horizontal rolls in the initiation of thunderstorms: A case study. *Mon. Weather Rev.*, **120,** 1785–1815